JOURNAL OF PROPULSION AND POWER
Vol. 27, No. 1, January–February 2011

Numerical Study on Turbulent Mixing of Spray Droplets in Crossflow

Bofeng Bai,* Huijuan Sun,† Haibin Zhang,† and Li Liu‡
Xi'an Jiaotong University, 710049 Xi'an, People's Republic of China

DOI: 10.2514/1.49826

A three-dimensional model for turbulent gas-droplet two-phase flow is developed to obtain a systematical understanding of the mixing process of centrifugal spray jet and turbulent crossflow in a horizontal tube. The turbulent dispersion and droplet-wall interaction are considered for modeling the dispersed phase in Lagrangian frame. The effects of influencing factors on the mixing process, including water/gas mass flow ratio, spray angle, droplet diameter, axial injection angle of spray nozzle and tangential injection angle of spray nozzle, are examined. Two indices, the degree of mixedness and the dimensionless droplet concentration, are proposed to assess the mixing performance of the spray droplets in the crossflow in a complementary way. The simulation results reveal that adding droplets into the crossflow imposes significant impact on the crossflow and in turn the affected crossflow produces considerable effect on dispersion and aggregation of the droplets. It is also found that the optimum mixing of droplets and crossflow can be achieved with the conditions that the water/gas mass flow ratio is 1:1, the spray angle is near 90°, the droplet diameter is larger, the axial injection angle of spray nozzle is 90°, and the tangential injection angle of spray nozzle is 0°.

Nomenclature

A_i = area of region i
C_D = drag coefficient
c_i = dimensionless droplet concentration
d_p = diameter of droplet
e = restitution coefficient
f = impinging droplet frequency
F_A = added mass force
F_D = aerodynamic drag force
F_g = gravitation
F_H = Basset force
$F_{L,M}$ = Magnus lift force
$F_{L,S}$ = Saffman lift force
F_S = pressure gradient force
G = turbulent energy production term
k = turbulent kinetic energy
N_i = the number of droplets passing through region i
n = the number of regions in the cross section
p = pressure of gas
Re_p = Reynolds number of droplet
S_ϕ^g = source terms due to gas
S_ϕ^p = source terms due to dispersed phase
u_i = time-average velocity of turbulent gas of i direction, $i = 1, 2$, and 3
u_i' = fluctuation velocity of turbulent gas of i direction, $i = 1, 2$, and 3
v_{an} = normal velocity of droplet after rebound from the wall
v_{at} = tangential velocity of droplet after rebound from the wall
v_{bn} = normal velocity of droplet before rebound from the wall
v_{bt} = tangential velocity of droplet before rebound from the wall
V_{nd} = normal velocity to the wall of the incident droplet
We = Weber number of droplet
X_i = flux density of droplets in region i
$\bar{X}$ = average flux density of droplets
Γ_ϕ = effective diffusion coefficient
ε = turbulent dissipation ratio
θ_i = injection angle of droplet from the wall
μ = dynamic viscosity of gas
μ_t = turbulent viscosity
ν = kinematic viscosity of droplet
ξ = degree of mixedness
ρ = density of gas
ρ_p = density of droplet
σ = surface tension of droplet
τ_p = velocity relaxation time
ϕ = 1, u_i, k, and ε

I. Introduction

MIXING of liquid or spray jets in crossflow is an interesting process that has found wide applications in many fields including internal combustion engine, humidifying performance of humid air turbine cycle [1], chemical processing industry, and manufacturing process of glass fibers [2]. Many theoretical and experimental efforts have been performed to study various mechanisms involved in the mixing process of liquid or spray jets in crossflow, such as, jet breakup, jet penetration, characteristics of spray droplets, interactions between jets and crossflow, vortex transportation, and heat and mass transfer phenomena. Liquid jet in crossflow is similar to gas jet in crossflow except that additional atomization of liquid jet would occur and is mainly dominated by momentum flux ratio. Inamura and Nagai experimentally investigated the spray characteristics of a liquid jet traversing subsonic airstreams [3]. They found that the waves on the liquid jet surface caused disintegration of the liquid jet and the droplet mean diameter diminished with the increasing of jet injection angle [4]. Fuller et al. [5] investigated the effect of injection angle on the breakup processes of liquid jet. The liquid column breakup behavior can be divided into two distinct regimes: aerodynamic and nonaerodynamic. Nouri and Whitelaw [6] measured the velocity and diameter of gasoline spray droplets in uniform crossflow and found that the momentum ratios of the bulk spray, flow regimes, vortical structure, droplet velocities,

Received 10 March 2010; revision received 3 October 2010; accepted for publication 4 October 2010.

*Professor, State Key Laboratory of Multiphase Flow in Power Engineering; bfbai@mail.xjtu.edu.cn.
†Ph.D. Candidate, State Key Laboratory of Multiphase Flow in Power Engineering; sunhuijuan@stu.xjtu.edu.cn.
‡Graduate Student, State Key Laboratory of Multiphase Flow in Power Engineering.

and droplet diameters were significantly affected by the crossflow properties. Kolář et al. [7] studied the vorticity transport within twin jets in crossflow (TJICF). The features of both tandem and side-by-side TJICF arrangements were examined and found to be strongly dependent on geometrical parameters. Ghosh and Hunt [8] examined the interactions between an external crossflow and a spray jet. They considered how fluid jets were deflected and deformed by crossflow to delineate the fluid mechanisms of spray in crossflow. Desantes et al. [9] studied the interaction between a turbulent gas jet/diesel spray with a crossflow. It was found that axis deflection and air entrainment were related to each other, and that the air/jet (or air/spray) momentum flux ratio was very relevant in the phenomena. Farooq et al. [10] investigated the drop size and velocity characteristics of sprays in a wind tunnel in the presence of a nonuniform crossflow. The presence of spray sheet created vortices in the crossflow and consequently affected the movement and velocity of spray droplets. Ariyapadi et al. [11] studied the spray characteristics of an industrial feed nozzle in the presence of a crossflow. It was found that the spray momentum flux affected the extent of jet bending and the spray droplets modified the structure of turbulence. Heat and mass transfer process is another main concern for the liquid spray in crossflow. It will not be elaborated in the present paper.

In recent years, water spray finds its new promising application in underwater propulsion systems, in particular, water ramjet. In the mixing chamber of water ramjet, the water is injected by the nozzles to a crossflow that is discharged from the combustion chamber. The spray evaporates in the crossflow at high temperatures and then the evaporated vapor mixes with the crossflow. On one hand, water spray assists to decrease the temperature of the fuel gas from the combustion chamber; on the other hand, the addition of water spray contributes to the increase of working substance that issues through the nozzle at the end of the water ramjet. Both a large temperature drop and a favorable mixing effect are able to enhance the propulsive power of the water ramjet. Therefore, it is of practical importance to investigate the mixing characteristics of water spray with crossflow with consideration of various factors to achieve an optimized propulsive performance of the water ramjet.

To the best of our knowledge, few researches have been reported on the mixing process in water ramjet. As the initial phase of the research, the phase change of water droplets is not considered and the mixing process in water ramjet is examined at cold states. The influencing factors of the mixing process include the ratio of spray and crossflow mass flux, the spray angle, the initial diameter of the spray droplets, and the injection mode of nozzles, etc. In our recent experiments [12], the injection mode of the nozzles was considered as the important factor that influenced the mixing effect. This study numerically investigates the effects of possible influencing factors on spray-crossflow mixing behaviors and provides a fundamental insight into the mixing characteristics of spray droplets in the crossflow in the presence of evaporation process.

II. Models and Mixedness Assessment Methods

A. Geometrical Structure

The geometrical layout of computation domain is shown in Fig. 1. The numerical simulation is conducted in a horizontal tube with a length of 560 mm and an inner diameter of 97.5 mm. Four pressure swirl nozzles are mounted at the same cross section of the tube that has a distance of 160 mm from the inlet. The hollow cone spray is injected into the tube through the swirl nozzles and then mixes with the crossflow. The Greek symbols, α and β, denote the axial and tangential injection angle of the nozzle, respectively. The coordinate system and the direction of gravity are also shown in Fig. 1. It should be noted that x/D denotes the ratio of distance in x direction to tube diameter. For instance, $x/D = 1.64$ indicates the cross section where the nozzles are positioned.

B. Computational Fluid Dynamics Models

The commercial computational fluid dynamics (CFD) software, FLUENT [13] is employed to simulate the mixing characteristics of spray droplets in the crossflow in the present work. With regard to the simulation of two-phase flow in the tube, the crossflow is treated as a continuous phase, for which the transport equations are solved by using the Eulerian approach. The spray droplets are treated as a dispersed phase, for which the transport equations are solved by using the Lagrangian approach.

1. Gas-Phase Equations

The gas-phase equations consist of conservation equations of mass and momentum if regardless of energy transfer. Based on the comparative analysis of standard k-ε model and realizable k-ε model, the standard k-ε model is applied to characterize the turbulence effect. The detailed explanation will be presented in Sec. III. The crossflow is assumed to be steady, incompressible and three-dimensional.

The equations of continuity, momentum can be written as

$$\rho \frac{\partial u_i}{\partial x_i} = 0 \tag{1}$$

$$\rho \frac{\partial (u_i u_j)}{\partial x_j} = -\frac{\partial p}{\partial x_i} + \frac{\partial}{\partial x_j}\left(\mu \frac{\partial u_i}{\partial x_j} - \rho \overline{u_i' u_j'}\right) + S_{u_i,p} \tag{2}$$

The Reynolds stress is expressed as

$$-\rho \overline{u_i' u_j'} = -\frac{2}{3}\rho k \delta_{i,j} + \mu_t \left(\frac{\partial u_i}{\partial x_j} + \frac{\partial u_j}{\partial x_i}\right) \tag{3}$$

where, the turbulent viscosity, μ_t, is described by

$$\mu_t = c_\mu \rho k^2 / \varepsilon \tag{4}$$

The transport equations for turbulent kinetic energy k and the dissipation rate ε are as follows:

$$\rho u_j \frac{\partial k}{\partial x_j} = \frac{\partial}{\partial x_j}\left[\left(\mu + \frac{\mu_t}{\sigma_k}\right)\frac{\partial k}{\partial x_j}\right] + \mu_t \frac{\partial u_i}{\partial x_j}\left(\frac{\partial u_i}{\partial x_j} + \frac{\partial u_j}{\partial x_i}\right) - \rho\varepsilon + S_{k,p} \tag{5}$$

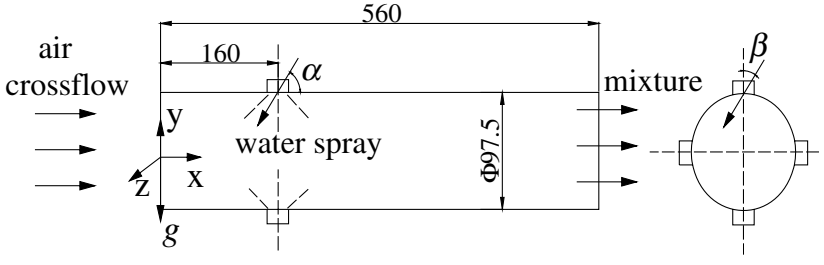

Fig. 1 Computation domain and coordinate system.

$$\rho u_j \frac{\partial \varepsilon}{\partial x_j} = \frac{\partial}{\partial x_j}\left[\left(\mu + \frac{\mu_t}{\sigma_\varepsilon}\right)\frac{\partial \varepsilon}{\partial x_j}\right] + \frac{c_1 \varepsilon}{k}\mu_t \frac{\partial u_i}{\partial x_j}\left(\frac{\partial u_i}{\partial x_j} + \frac{\partial u_j}{\partial x_i}\right) - c_2 \rho \frac{\varepsilon^2}{k} + S_{\varepsilon,p} \tag{6}$$

where the usual turbulence energy production term G is defined as

$$G = \mu_t \frac{\partial u_i}{\partial x_j}\left(\frac{\partial u_i}{\partial x_j} + \frac{\partial u_j}{\partial x_i}\right) \tag{7}$$

All the governing equations can be unified as

$$\frac{\partial}{\partial x_j}(\rho u_j \phi) = \frac{\partial}{\partial x_j}\left(\Gamma_\phi \frac{\partial \phi}{\partial x_j}\right) + S_\phi^g + S_\phi^p \tag{8}$$

where S_ϕ^g and S_ϕ^p are the source terms due to gas and dispersed phase.

2. Dispersed Phase Equations

The formation of liquid film, the breakup process of spray sheet, and the generation of droplets are not taken into account. The hollow cone spray shape and the Sauter diameter of the droplets are considered. The pressure swirl spray model, named as the linearized instability sheet atomization (LISA) model by Schmidt et al. [14], is applied to add droplets into the crossflow. The atomization process involves breakup, collision, and coalescence of droplets. The well-known TAB breakup model [15] is used since it is appropriate for predicting secondary breakup regime in the jet process at low We number. O'Rourke's statistical particle method [16], for which parcels of droplets can be tracked in a three-dimensional space and simultaneously with time, is used to simulate the collision and coalescence process of droplets. The detailed models refer to the FLUENT user manual.

The droplet trajectories are calculated in a Lagrangian framework. The forces acting on the droplets can be generally classified to aerodynamic drag force, gravitation force, force due to added mass, force due to gas-phase pressure gradient, Basset history integral force, Saffman and Magnus lift force. Summation of these forces leads to the following equation

$$\sum F = F_D + F_g + F_A + F_S + F_H + F_{L,S} + F_{L,M} \tag{9}$$

The Basset force acting on the particles can be neglected in the turbulent flow. The Saffman and Magnus lift force can also be neglected in the case of small velocity gradient in the main flow [17]. Furthermore, the forces except drag and volume forces are negligible when the gas/particle density ratio is smaller than 10^{-3} [18]. Therefore, the forces F_A, F_S, F_H, $F_{L,S}$, and $F_{L,M}$ are neglected in this study. The aerodynamic drag force and gravitation force are considered. The droplets are assumed to be spherical. The motion of the droplets is described by

$$\frac{\mathrm{d}\mathbf{u}_p}{\mathrm{d}t} = (\mathbf{u}_g - \mathbf{u}_p)/\tau_p + \mathbf{g} \tag{10}$$

$$\tau_p = \frac{24 \rho_p d_p^2}{18 \mu C_D Re_p} \tag{11}$$

$$Re_p = \frac{\rho_g |\mathbf{u}_g - \mathbf{u}_p| d_p}{\mu} \tag{12}$$

$$C_D = \left(\frac{24}{Re_p}\right)(1 + 0.15 Re_p^{0.687})(Re_p < 1000)$$
$$C_D = 0.44(Re_p \geq 1000) \tag{13}$$

The turbulence effect is simulated by using the stochastic droplet tracking method, in which the instantaneous velocity of gas phase is decomposed into a mean and fluctuating component

$$V = \bar{V} + V' \tag{14}$$

where $\bar{V}$ is determined through solving gas-phase equations and V' is sampled randomly from a Gaussian probability distribution of gas-phase velocity.

With regard to the interaction of droplet and wall, Bai and Gosman [19] identified seven impingement regimes that include stick, spread, rebound, rebound with breakup, boiling-induced breakup, breakup, and splash. However, this classification appears to be rather complex. The transition criteria of four regimes involving stick, rebound, spread and splash when the wall temperature is less than the liquid boiling temperature are proposed by Stanton and Rutland [20] based on the We number

$$We = \frac{\rho_p d_p V_{nd}^2}{\sigma} \tag{15}$$

1) $We < 5$, for stick regime, 2) $5 < We < 10$, for rebounding regime, 3) $10 < We < 18.0^2 d_p (\frac{\rho}{\sigma})^{\frac{1}{2}} \nu^{\frac{1}{4}} f^{\frac{3}{4}}$, for spreading regime, and 4) $We > 18.0^2 d_p (\frac{\rho}{\sigma})^{\frac{1}{2}} \nu^{\frac{1}{4}} f^{\frac{3}{4}}$, for splashing regime.

In the scope of present study, very few droplets demonstrate a Weber number larger than 10. Therefore, the droplet-wall interaction model can be simplified as follows.

1) $We < 5$, the droplet escapes from the wall. Accordingly, the calculation of droplet trajectory stops.

2) $5 < We < 10$, the droplet rebounds from the wall and the normal (v_{an}) and tangential (v_{at}) velocity after rebound are calculated by

$$v_{an} = -e v_{bn} \tag{16}$$

$$v_{at} = \frac{5 v_{bt}}{7} \tag{17}$$

where e can be calculated by the following equation proposed by Bai and Gosman [19]

$$e = 0.993 - 1.76\theta_i + 1.56\theta_i^2 - 0.49\theta_i^3 \tag{18}$$

3) $We > 10$, the droplet is trapped by the wall, indicating that the calculation of droplet trajectory ends.

The source term S_ϕ^p represents the term due to adding particles into the crossflow. Table 1 provides a summary of source terms encountered in the mixing process of spray droplets in a crossflow.

The turbulence model constants, c_μ, c_1, c_2, c_3, σ_k, and σ_ε, are determined as 0.09, 1.44, 1.92, 1.87, 1.0, and 1.3, respectively.

Table 1 Summary of the source terms

ϕ	Γ_ϕ	S_ϕ^g	S_ϕ^p
1	——	——	——
u_i	$\mu + \mu_t$	$-\frac{\partial}{\partial x_i}(p + \frac{2}{3}\rho k) + \frac{\partial}{\partial x_j}\left(\mu_t \frac{\partial u_j}{\partial x_i}\right) + \rho g_i$	$-\sum_p \frac{\dot{m}_p N_p}{V_{i,j}}\left[\left(u_{j,p}^{t+\Delta t} - u_{j,p}^t\right) - g_i \Delta t\right]$
k	$\mu + \frac{\mu_t}{\sigma_k}$	$G - \rho\varepsilon$	$\overline{u_j S_{u_j}} - \bar{u}_j \overline{S_{u_j}}$
ε	$\mu + \frac{\mu_t}{\sigma_\varepsilon}$	$\frac{\varepsilon}{k}(c_1 G - c_2 \rho\varepsilon)$	$c_3 \frac{\varepsilon}{k} \bar{S}_k$

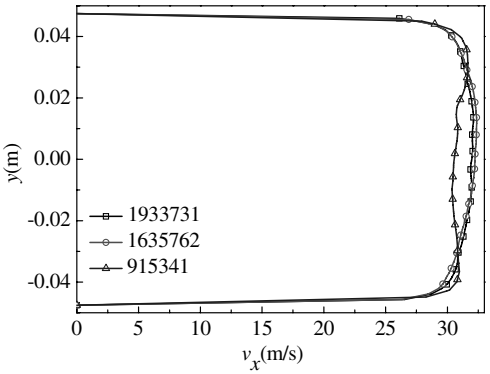

Fig. 2 Grid-dependence checks of simulation results.

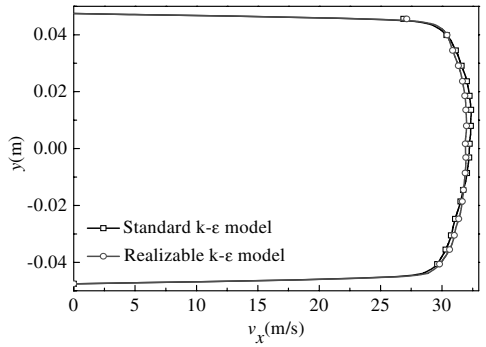

Fig. 3 Turbulent model for gas-phase comparison.

C. Mixedness Assessment Method

Several popular mixing indices have been employed to describe the mixing effectiveness in the processing industry [21]. Most of these indices are developed based on statistical analysis and especially on the definitions of standard deviations of a specified property [22]. Because of its simplicity, the well-known Lacey index is widely used in the processing industry [23]. The concept of degree of mixedness or mixing coefficient has been also used for describing pollutant dispersion processes in rivers, mixing process of particle system in fluidized bed, inline jets to crossflow in t gas turbine combustion, etc. Chaikittisilp et al. [24] analyzed the solid particle mixing in inclined fluidized beds. The mixing index, degree of mixedness, was assessed by evaluating the magnitude of the sample variance. Since the jet concentration is a key parameter to define spatial unmixedness [25,26], the spatial unmixedness is much more applicable for two-stream mixing problem. Spray quality is another comprehensive parameter that takes into account the Sauter diameter D_{32}, extend of area of spray EA, and spatial unmixedness U_s [27]. Spray quality was originally proposed to assess the spray quality of airblast. Although this parameter was employed to assess the required spray characteristics of nozzles instead of the mixedness, it provided an exemplary evaluation of the mixedness with the consideration of various influencing factors. One of the current research objectives is to obtain a desired even distribution of liquid droplets at any given position along the mixing tube. The abovementioned proposed definitions of degree of mixedness vary from each other in terms of applicability. With regard to the unique mixing process discussed in the present study, two assessment indices are proposed to evaluate the mixing process complementarily.

The degree of mixedness is used to describe the mixing characteristics of droplets and crossflow in certain cross section. The cross section is divided into some smaller regions, where statistical certainty of the number of droplets can be obtained by determining the 2-D coordinate of every droplet. Furthermore, the flux density of droplets in each region, X_i, and the mean flux density,$\bar{X}$, in the cross section can be obtained. The degree of mixedness is proposed as

$$\xi = 1 - \frac{\frac{1}{n-1}\sum_{i=1}^{n}(X_i - \bar{X})^2}{\bar{X}^2} \tag{19}$$

The flux density indicates the number of droplets per unit area. For instance, if there are N_i droplets passing through the region with the area of A_i, the flux density of the region i is

$$X_i = \frac{N_i}{A_i} \tag{20}$$

The definition of the degree of mixedness is derived based on variance. Its maximal value is 1, representing an ideal mixing state. A smaller value indicates a worse state of mixing which suggests the uneven distribution of droplets in the cross section.

Moreover, the dimensionless droplet concentration defined by Eq. (21) can be used to draw isoconcentration lines in the cross section

$$c_i = \frac{X_i}{\overline{X}} \tag{21}$$

III. Numerical Implementation and Computation Conditions

The governing equations for gas phase and discrete phase are discretized on a hybrid grid system. Tetrahedral meshes with a large concentration of nodes are used in the vicinity of nozzles and prismatic meshes in the regions far from the nozzles are employed. Comparison of x-direction crossflow velocity by using different number of grids is made to assess grid-dependence of simulation

Table 2 Computing conditions for 16 simulation cases

Case	Water/gas mass flow ratio	Sauter diameter, μm	Spray angle, °	Axial injection angle, °	Tangential injection angle, °
1	1:1	100	120	90	0
2	1.5:1	100	120	90	0
3	1.7:1	100	120	90	0
4	2:1	100	120	90	0
5	1:1	100	60	90	0
6	1:1	100	80	90	0
7	1:1	100	90	90	0
8	1:1	100	100	90	0
9	1:1	120	120	90	0
10	1:1	60	120	90	0
11	1:1	100	120	60	0
12	1:1	100	90	80	0
13	1:1	100	90	100	0
14	1:1	100	120	120	0
15	1:1	100	120	90	10
16	1:1	100	120	90	20

results. It is found in Fig. 2 that the effect of grid quantity on simulation results can be ignored when the grid quantity exceeds about 1,600,000.

The gas-phase equations are solved by using a control-volume technique that is available in the SIMPLE algorithm. The droplet parcels are introduced in a form of hollow cone spray by pressure swirl nozzles. The calculation procedure is: 1) a converged solution of the gas flowfield is calculated without considering the source terms for the dispersed phase; 2) a large number of discrete parcels are traced throughout the flowfield and average values of the source terms are evaluated. In the atomization process, the breakup, collision and coalescence of droplets are considered; and 3) the flowfield is updated by considering the source terms for the dispersed phase. Although the statistical diameter D_{32} is used, the practical droplet size ranges approximately from 20 μm to 100 μm. The minimum eddy life time and residence time of the minimum droplet, 1e-4s, is used as the time step of iteration. And the crossflow velocity and grid size are comprehensively considered to determine the time step.

The inlet velocity, inlet turbulence intensity, and temperature of the used gas crossflow are 35 m/s, 3.48%, and 20°C, respectively. The operating pressure in the tube is maintained from 2 to 3 MPa. The water mass flux from a single nozzle is 0.0659 kg/s. A no-slip boundary condition is imposed on the velocity components at the wall. Calculation results by using the standard k-ε model and realizable k-ε model for the gas phase are compared. As Fig. 3 shows, the standard k-ε model can satisfy the computation requirements. The hollow cone spray is used to generate an initial droplet distribution since it does not bring about a strong swirling in the tube. It is worth noting that no strong swirling flow is observed either in the experiments or in the calculations.

The working conditions for different simulation cases are shown in Table 2.

IV. Results and Discussion

A. Validation with Experiments

The numerical algorithm and computed results are validated by comparing the simulated results with the experimental results conducted by the authors. A rectangular duct with a 95 × 95 mm cross section instead of a circular tube was used in the experiments since it is difficult to obtain images of the turbulent mixing phenomenon in a circular tube. Moreover, two nozzles, instead of four nozzles used in the simulations, were used in the experiments to

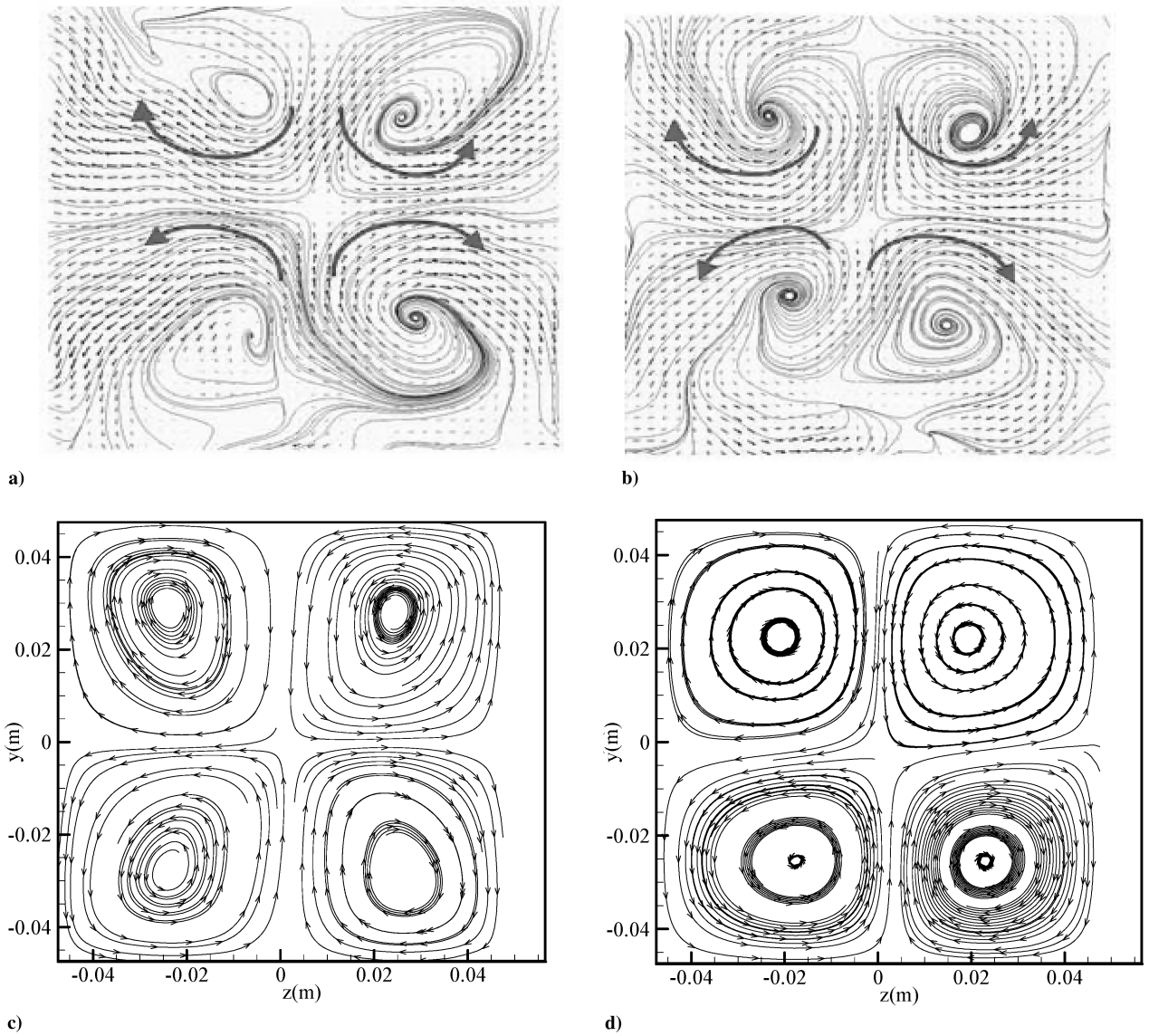

Fig. 4 Comparison of experimental and calculated gas-phase streamline under the influence of droplets: a) experimental gas-phase streamline at a cross section 100 mm downstream of the nozzles; b) experimental gas-phase streamline at a cross section 220 mm downstream of the nozzles; c) calculated gas-phase streamline at the cross section 100 mm downstream of the nozzles; and d) calculated gas-phase streamline at the cross section 220 mm downstream of the nozzles.

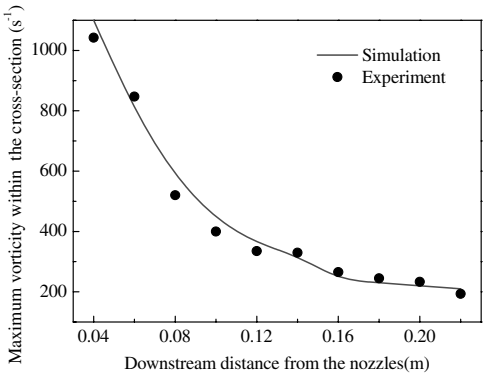

a)

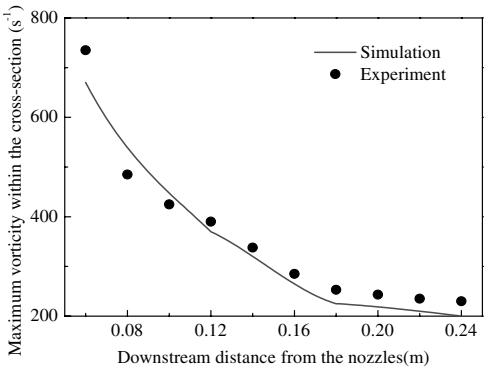

b)

Fig. 5 Comparison of experimental and calculated vorticity profiles at different cross section along the crossflow: a) the Reynolds number of gas phase is 25,700; and b) the Reynolds number of gas phase is 45,000.

achieve clearer transient images. The experiments used two values of Reynolds number, 25,700 and 45,000, which corresponded to 4 and 7 m/s of gas inlet velocity, respectively. The injection angle of spray nozzles is set as 90°. More experimental details can be found elsewhere [28,29]. Figures 4 and 5 compare the flow structure and vorticity at different cross section obtained from the experiments and the simulations. It can be observed from Fig. 4 that two counter-rotating vortex pairs (CVP) are produced owing to the interactions between the crossflow and the spray jet. The CVP can hold within a certain distance and keep stable in configuration, while the energy of the vortex attenuates along the crossflow as shown in Fig. 5. It is demonstrated from Figs. 4 and 5 that the gas-phase flowfields achieved from the experiment agree well with that from the simulation. The maximal error between the experiment and

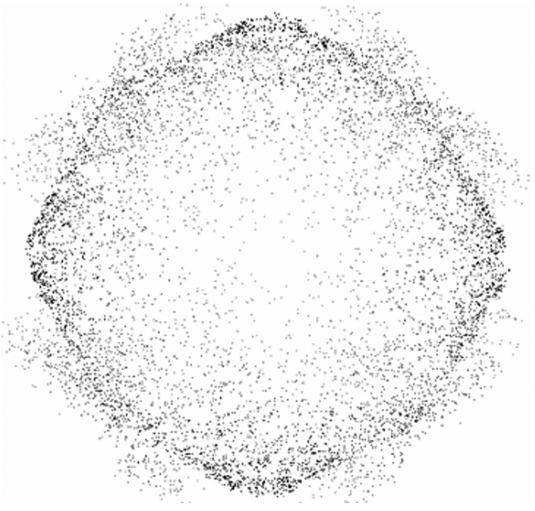

Fig. 6 Flow structure of droplets from the four nozzles.

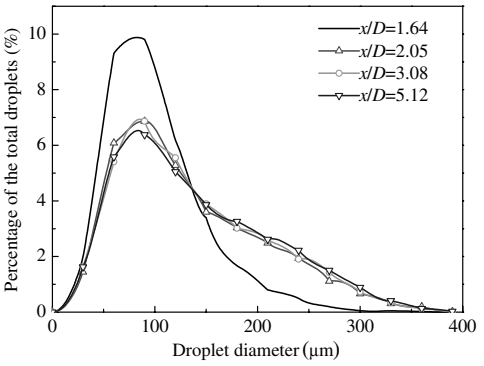

Fig. 7 Distribution of droplet diameter at different cross section with $x/D = 1.64$, 2.05, 3.08, and 5.13.

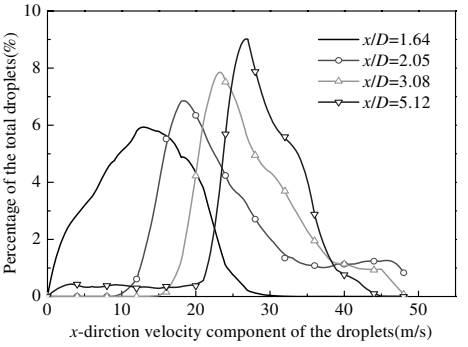

a)

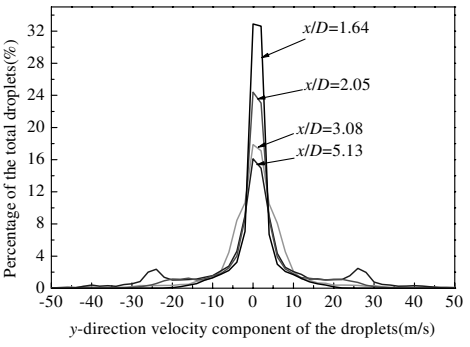

b)

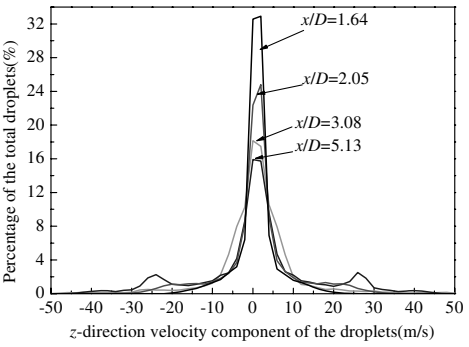

c)

Fig. 8 Distribution of velocity component of droplets at different cross section of $x/D = 1.64$, 2.05, 3.08 and 5.13: a) the axial, i.e., x-direction, velocity component; b) the y-direction velocity component; and c) the z-direction velocity component.

simulation is 12% in Fig. 5b. For different conditions, the simulation can agree well with the experiment.

B. Overview of Droplet Characteristics

Before proceeding with further discussion and analysis, it is necessary to examine the droplet size, droplet velocity, and the flow structure at the outlet of nozzles.

The flow structure of droplets from the pressure swirl nozzles is shown in Fig. 6. The mixing of droplets in crossflow can be affected by the initial distribution of droplets. Figure 7 shows the droplet size distributions at different cross section. The diameter of most droplets at the outlet of nozzles approaches to 100 μm. At the downstream of the nozzles, however, the droplet diameter tends to show larger value and covers a wide range. The three figures in Fig. 8 show the distribution of droplet velocity along the crossflow. The axial velocity of droplets from the nozzles is mainly between 5 and 20 m/s. With the motions of droplets, the velocities of droplets increase to follow the main flow, the majority of which can reach 25–35 m/s at $x/D = 5.13$.

C. Effect of Addition of Droplets on the Flowfield

Figure 9 presents the turbulence intensity in different cross section for case 7 in Table 2. The turbulence intensity has a sharp increase in the vicinity of the nozzles and a relatively slight increase at locations far from the nozzles. At the cross section near the nozzle, the increment of turbulence intensity near the wall is much larger than that in the center region of the tube. However, the difference of turbulence intensity in different cross section far from the nozzles tends to be moderate. It can be ascribed to the fact that the main flowfield near the nozzles is significantly affected by the disturbance introduced by the droplets, resulting in an intensified turbulence. The disturbance due to droplet addition also results in a larger fluctuation of gas velocity, which in turn promotes the dispersion of droplets.

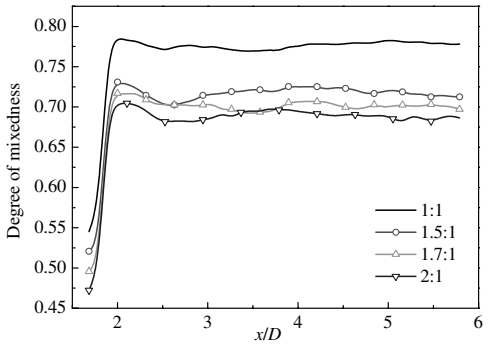

Fig. 11 Degrees of mixedness at different water/gas mass flow ratios (for case 1, 2, 3, and 4 in Table 2).

This disturbance tends to fade downstream and shows less effect on the crossflow.

Figure 10 illustrates the development of four counter-rotating vortex pairs along the crossflow. It can be clearly observed from Fig. 10 that the four counter-rotating vortex pairs originate near the wall and attenuate along the streamwise direction. The vortex pairs caused by mutual interactions between droplets and crossflow can account for the enhancement of turbulence. Comparison of Figs. 9 and 10 also reveals that the location where turbulence intensity increases substantially is where a large vortex pair develops. The vortex pairs promote the dispersion of droplets and meanwhile cause regionally intensified turbulence.

D. Effect of Water/Gas Mass Flow Ratio on Mixedness

Figure 11 shows the degrees of mixedness at different water/gas mass flow ratios. It can be seen in Fig. 11 that the degree of mixedness at different water/gas mass flow ratios have similar characteristics.

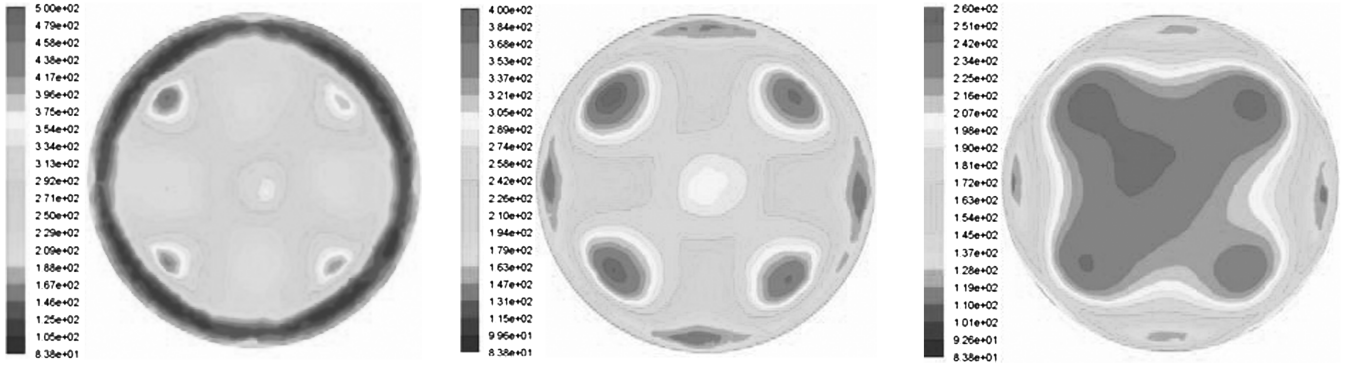

a) b) c)

Fig. 9 Turbulence intensity for case 7 in Table 2 at different cross section of: a) $x/D = 1.64$; b) $x/D = 2.05$; and c) $x/D = 3.08$.

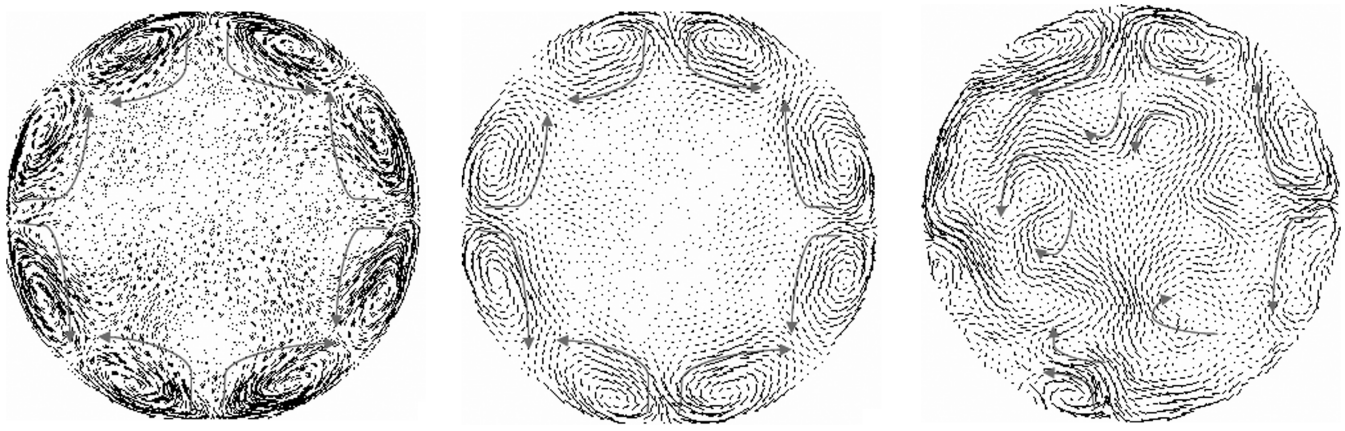

a) b) c)

Fig. 10 Velocity vector of gas phase for case 7 in Table 2 at different cross section with: a) $x/D = 1.64$; b) $x/D = 2.05$; and c) $x/D = 4.1$.

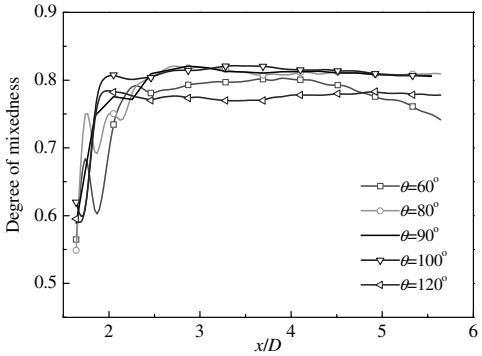

Fig. 12 Degrees of mixedness at different spray angles (for case 1, 5, 6, 7, and 8 in Table 2).

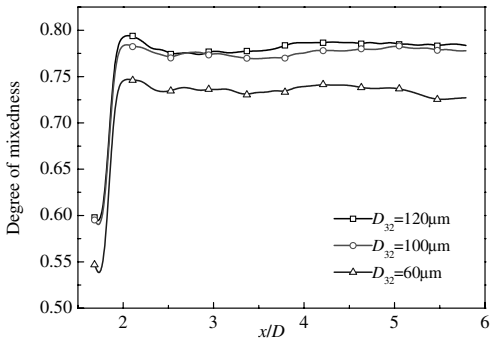

Fig. 14 Degrees of mixedness for different Sauter mean diameters (for case 1, 9, and 10 in Table 2).

With the spanwise dispersion of droplets, the degree of mixedness increases rapidly and tends to be stable after a short mixing distance. Herein it is assumed that the droplets are thoroughly mixed with the crossflow when the degree of mixedness reaches a satisfactorily stable value. Maxey [30] used asymptotic methods to demonstrate that the effect of inertia was to cause dense particles to accumulate in regions of low vorticity and high strain rate.

As shown in Fig. 11, better mixing effect can be achieved at a lower water/gas mass flow ratio. With the gas flow rate being constant, a higher water/gas mass flow ratio results in a higher water

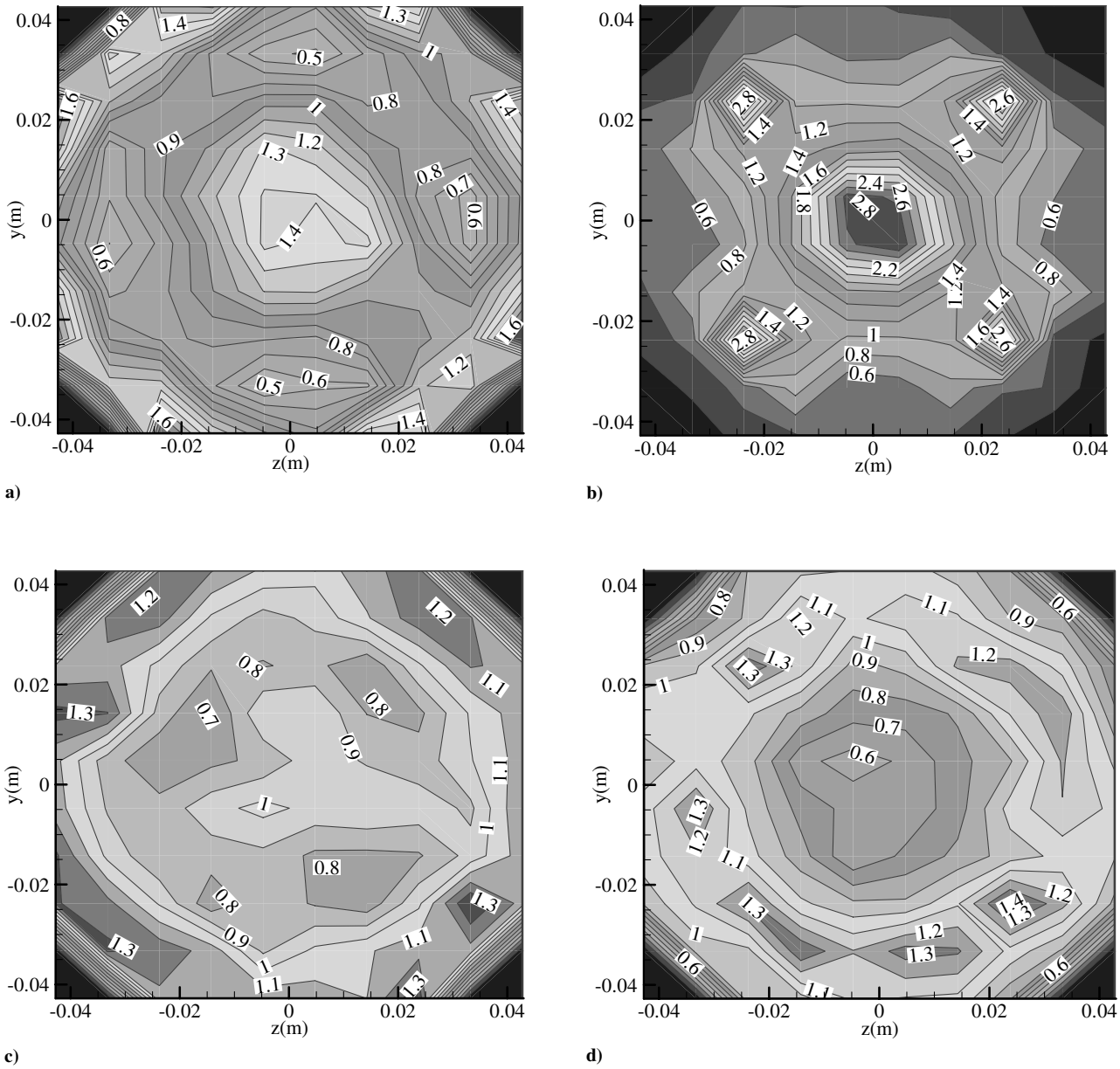

Fig. 13 Isoconcentration contour lines of droplet at: a) $\theta = 120°$ and $x/D = 1.64$; b) $\theta = 90°$ and $x/D = 1.64$; c) $\theta = 120°$ and $x/D = 5.13$; and d) $\theta = 90°$ and $x/D = 5.13$. (θ denotes the spray angle.)

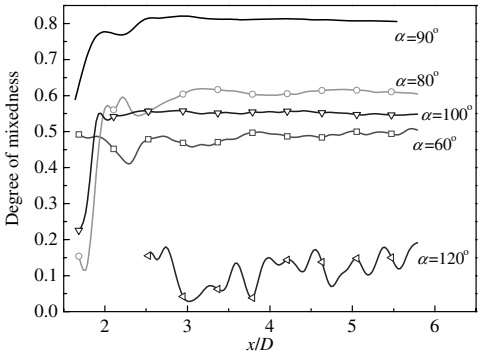

Fig. 15 Degrees of mixedness for different axial injection angles (for case 7, 11, 12, 13 and 14 in Table 2).

flow rate, a higher initial droplet velocity, a larger disturbance to gas phase, a greater eddy size and a delayed eddy development. Nevertheless, these effects are unfavorable for the mixing of droplets and gas crossflow. Fung and Perkins [31] found that there was a possibility that particles might become trapped within eddies for certain ratios of particle time constant to fluid time scale. The droplets rotate toward periphery of the eddy due to centrifugation effect, resulting in that the droplets around the eddy periphery are denser than in other zones. Squires and Eaton [32] also demonstrated that the uneven distribution of droplets could be accounted for by the preferential concentration of the particles in the eddy.

E. Effect of Spray Angle on Mixedness

The degrees of mixedness for five spray angles are shown in Fig. 12. The degree of mixedness increases with the increase of spray angle given that the angle is less than 90°, while decreases as the spray angle increases when the angle is greater than 90°. The degrees of mixedness for spray angles of 80, 90, and 100° do not show much difference with each other and are considered to be the optimum scenarios. As shown in Fig. 13, the droplets at the cross section with x/D of 1.64, where the nozzles are mounted, tend to congregate in the tube center and the space between two adjacent nozzles. This phenomenon is pronounced for the spray angle of 90°, which can be explained by the cone spray shape and the presence of large eddy. On one hand, the droplets in the tube center for spray angle of 120° are scarcer than that for 90° since the droplets are mainly generated

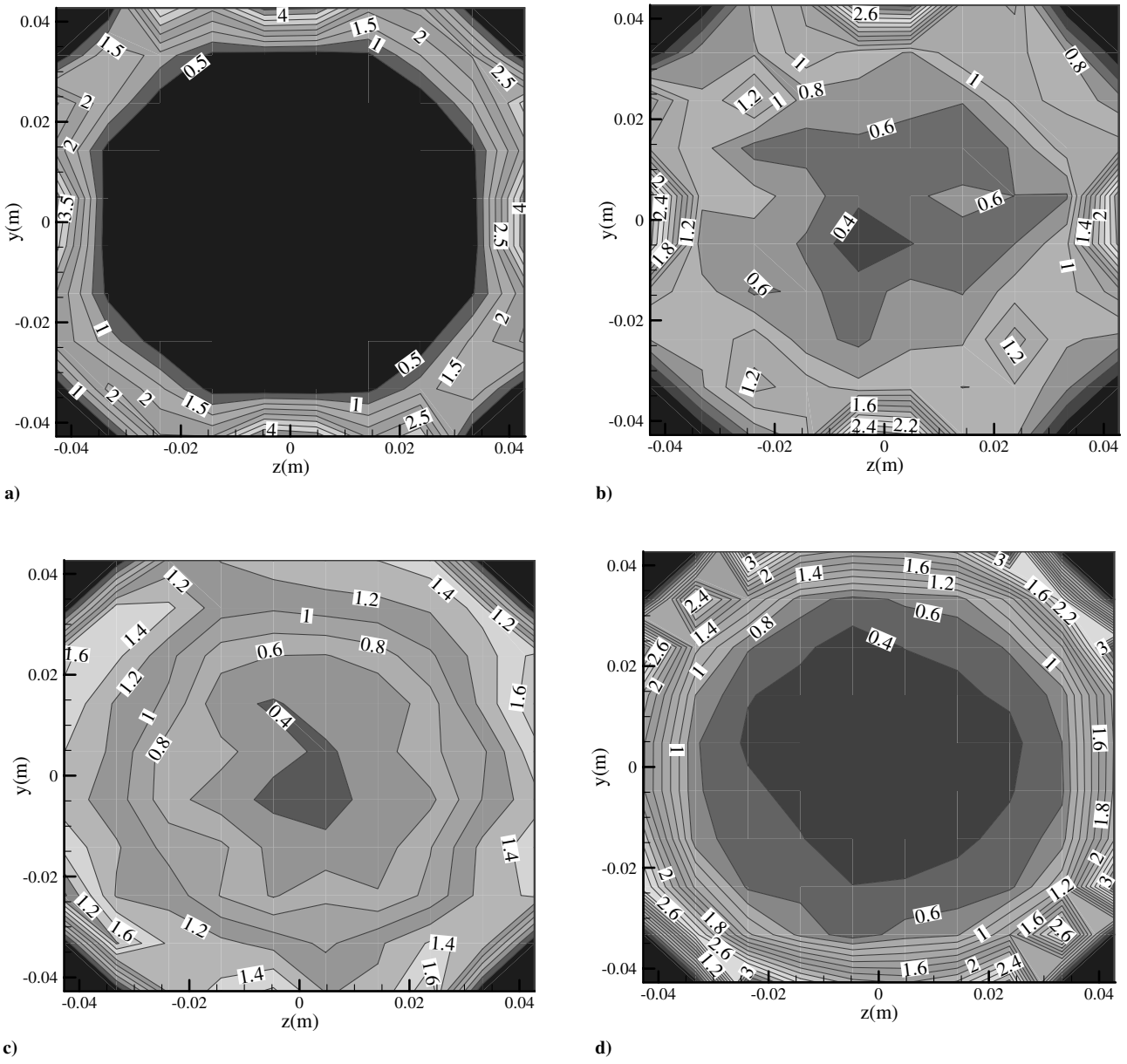

Fig. 16 Isoconcentration contour lines of droplets at: a) $\alpha = 60°$ and $x/D = 1.64$; b) $\alpha = 120°$ and $x/D = 1.64$; c) $\alpha = 60°$ and $x/D = 4.1$; and d) $\alpha = 120°$ and $x/D = 4.1$.

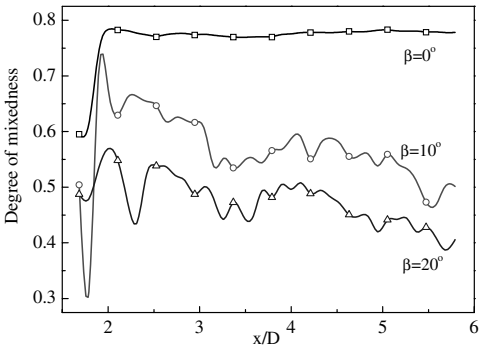

Fig. 17 Degrees of mixedness for different tangential injection angles (for case 1, 15, and 16 in Table 2).

around the peripheries of the cone spray. On the other hand, the droplets concentrate at the places where large eddies occur, as Fig. 13 shows. Big droplets with relatively large inertia may easily go through small eddies since small eddies have little influence on the movement of big particles. At the cross section with x/D of 5.13, the dimensionless concentration in every part of the cross section approaches to the average concentration.

F. Effect of Droplet Size on Mixedness

The statistical diameter, Sauter mean diameter, is used to characterize the mean diameter of the bulk droplets. The effect of Sauter mean diameter on the degree of mixedness is shown in Fig. 14. The degree of mixedness with Sauter diameter of 60 μm is much lower that with Sauter diameter of 120 μm, while the degree of mixedness with Sauter diameter of 100 μm is similar to that with Sauter diameter of 120 μm. Therefore, it can be deduced that the effect of droplet diameter on mixedness can be neglected when the Sauter diameter of the droplets increases to a certain value. The movement of droplets with small diameter can be easily disturbed by eddy and hence the small droplets tend to accumulate due to centrifugation effect, resulting in a relatively lower degree of mixedness. The eddy has little influence on the movement of big droplets since big droplets possess larger inertia.

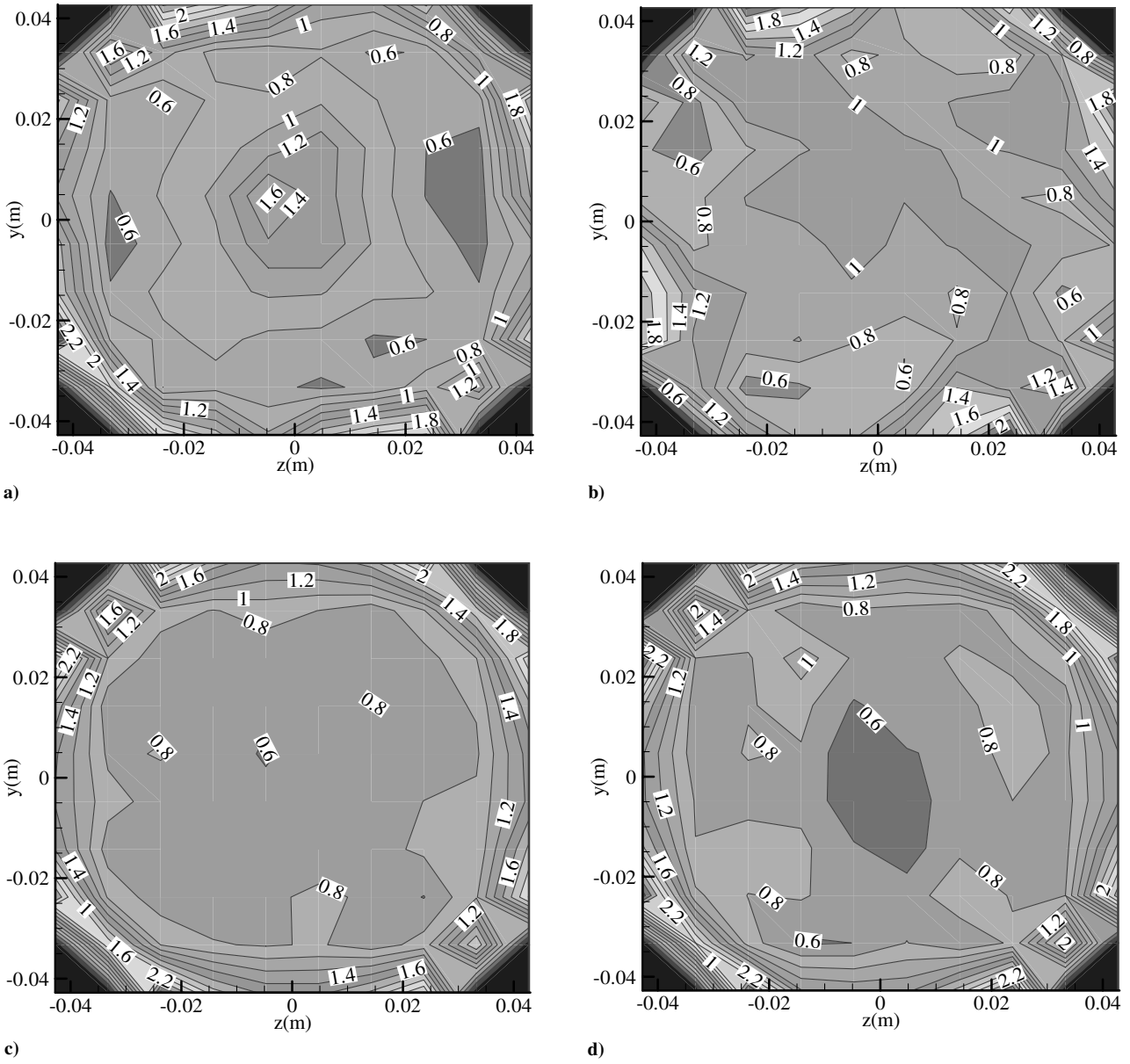

Fig. 18 Isoconcentration contour lines of droplets at: a) $\beta = 10°$ and $x/D = 1.64$; b) $\beta = 20°$ and $x/D = 1.64$; c) $\beta = 10°$ and $x/D = 5.13$; and d) $\beta = 20°$ and $x/D = 5.13$.

G. Effect of Axial Injection Angle of Nozzles on Mixedness

As Fig. 1 shows, the axial and tangential injection angles are denoted by the symbol α and β, respectively. Figure 15 shows the calculated degree of mixedness when the axial injection angles are 60, 80, 90, 100, and 120°.

As shown in Fig. 15, the optimum degree of mixedness is obtained with the axial injection angle of 90°. It can be also seen that the degree of mixedness with an axial injection angle smaller than 90° is more desirable than that with an injection angle larger than 90°. Figure 16 compares the calculated isoconcentration contour lines of droplets at two cross sections for the cases of $\alpha = 60$ and $\alpha = 120°$. As can be seen in Fig. 16a, the droplets have a strong tendency of congregating in the vicinity of the tube wall when the injection angle is much smaller than 90°. The similar phenomenon is observed when the injection angle is much larger than 90°, as illustrated in Fig. 16d. It is reasonable to speculate that when the axial injection angles are 0 and 180°, majority of the spray droplets would concentrate near the wall and as a result the degrees of mixedness for these axial injection angles would be fairly low. An explanation why the axial injection angles of 80 and 60° fail to generate satisfactory mixedness is as follows. First, the droplets in the upstream flow of the nozzles in the near-wall region account for a large fraction, which influences the droplets distribution as Fig. 16a shows. Second, the eddy attenuates quickly downstream because the mixing process occurs in advance. The large droplet is not readily affected by the small eddy and manages to keep the current trajectory direction. Third, the average axial velocity of the droplets is much greater than the other two velocity components. The low lateral velocities results in weak spanwise dispersion of the dispersed phase. The above reasons account for the relatively low degree of mixedness for the injection angle of 80 and 60°. For the case of 120° axial injection angle, the small normal and tangential velocity components are not sufficient to produce entrainment effect and large eddies. Moreover, the hollow cone spray shape and short mixing distance are unfavorable for the satisfactory mixedness.

H. Effect of Tangential Injection Angle of Nozzles on Mixedness

Figure 17 shows the effect of tangential injection angle of nozzles on the mixing effect. In general, it can be seen from Fig. 17 that the degree of mixedness decreases with the increase of the tangential injection angle. Figure 18 illustrates the calculated isoconcentration contour lines at two cross sections for the cases of $\beta = 10°$ and $\beta = 20°$, respectively. Figures 18a and 18b suggest that a large tangential injection angle provides an adverse initial condition of the mixing process where most of the droplets are near the tube wall. In addition, the degree of mixedness even deteriorates with the mixing process going on, as shown by Figs. 18c and 18d. It can be concluded that the optimum degree of mixedness can be achieved with unbiased injection angles of nozzles.

V. Conclusions

Numerical simulations of the mixing behavior of spray droplets in a gas crossflow have been conducted in this study with consideration of various influencing factors. The simulation results are proven to be reliable by validating them to experimental data. It is observed in both experiments and simulations that counter-rotating vortex pairs are generated by the adding spray droplets into the gas crossflow, which significantly enhances the turbulence intensity of the gas phase. The large eddies that appear in the vicinity of nozzles also contribute to the remarkable increase of turbulence intensity of the gas phase. Along the streamwise direction, the increment of turbulence intensity of the gas phase decreases gradually with the attenuation of eddy energy and the fading disturbance of droplets to the crossflow. The entrainment effect and centrifugation effect caused by the large eddies lead to an uneven distribution of droplets in the vicinity of the spray, resulting in a low degree of mixedness. In general, the degree of mixedness increases rapidly to reach a relatively high value at cross sections that are located downstream of the nozzles. Meanwhile, the droplets tend to aggregate in the near-wall region for all the cases simulated owing to both the shape of hollow cone spray and the droplets' tendency to congregating in high-strain and low-vortex regions.

Two indices, the degree of mixedness and the dimensionless droplet concentration, have been proposed to assess the mixing effectiveness of the spray droplets in the crossflow in a complementary way. Within the scope of this study, the optimum degree of mixedness is achieved with a water/gas mass flow ratio of 1:1 and a spray angle of near 90°. The degree of mixedness for spray droplets with larger diameter is greater than that for small-size droplets. An unbiased injection of spray through pressure swirl nozzles provides the most favorable degree of mixedness. An axial injection angle smaller than 90° results in a higher degree of mixedness than that greater than 90°. Moreover, the degree of mixedness decreases with the increase of the tangential injection angle.

Acknowledgment

This work was financially supported by the National Nature Science Foundation of China for Creative Research Groups under the Contract No. 50821064.

References

[1] Wang, Y. Z., Li, Y. X., Weng, S. L., and Wang, Y. H., "Numerical Simulation of Counter-Flow Spray Saturator for Humid Air Turbine Cycle," *Energy*, Vol. 32, No. 5, 2007, pp. 852–860. doi:10.1016/j.energy.2006.05.008

[2] Eletribi, S., "Dispersion of Water Sprays in a Transverse Air Jet and the Aging of Spray Nozzles," Massachusetts Institute of Technology, 1999.

[3] Inamura, T., and Nagai, N., "Spray Characteristics of Liquid Jet Traversing Subsonic Airstreams," *Journal of Propulsion and Power*, Vol. 13, No. 2, 1997, pp. 250–256. doi:10.2514/2.5156

[4] Costa, M., Melo, M. J., Sousa, J. M. M., and Levy, Y., "Spray Characteristics of Angled Liquid Injection into Subsonic Crossflows," *AIAA Journal*, Vol. 44, No. 3, 2006, pp. 646–653. doi:10.2514/1.10887

[5] Fuller, R. P., Wu, P. K., Kirkendall, K. A., and Nejad, A. S., "Effects of Injection Angle on Atomization of Liquid Jets in Transverse Airflow," *AIAA Journal*, Vol. 38, No. 1, 2000, pp. 64–72. doi:10.2514/2.923

[6] Nouri, J. M., and Whitelaw, J. H., "Gasoline Sprays in Uniform Crossflow," *Atomization and Sprays*, Vol. 17, No. 7, 2007, pp. 621–640. doi:10.1615/AtomizSpr.v17.i7.30

[7] Kolář, V., Takao, H., Todoroki, T., Savory, E., Okamoto, S., and Toy, N., "Vorticity Transport within Twin Jets in Crossflow," *Experimental Thermal and Fluid Science*, Vol. 27, No. 5, 2003, pp. 563–571. doi:10.1016/S0894-1777(02)00270-4

[8] Ghosh, B. S., and Hunt, J. C. R., "Spray Jets in a Cross-flow," *Journal of Fluid Mechanics*, Vol. 365, No. 1, 1998, pp. 109–136. doi:10.1017/S0022112098001190

[9] Desantes, J. M., Arrègle, J., López, J. J., and García, J. M., "Turbulent Gas Jets and Diesel-Like Sprays in a Crossflow: a Study on Axis Deflection and Air Entrainment," *Fuel*, Vol. 85, Nos. 14–15, 2006, pp. 2120–2132. doi:10.1016/j.fuel.2006.03.025

[10] Farooq, M., Balachandar, R., Wulfsohn, D., and Wolf, T. M., "PA-Precision Agriculture: Agricultural Sprays in Cross-flow and Drift," *Journal of Agricultural Engineering Research*, Vol. 78, No. 4, 2001, pp. 347–358. doi:10.1006/jaer.2000.0660

[11] Ariyapadi, S., Berruti, F., and Balachandar, R., "Effect of Cross Flow on the Spray Characteristics of an Industrial Feed Nozzle," *Chemical Engineering Communications*, Vol. 190, No. 12, 2003, pp. 1681–1704. doi:10.1080/713711187

[12] Bai, B. F., Zhang, H. B., Liu, L., and Sun, H. J., "Experimental Study on Turbulent Mixing of Spray Droplets in Crossflow," *Experimental Thermal and Fluid Science*, Vol. 33, No. 6, 2009, pp. 1012–1020. doi:10.1016/j.expthermflusci.2009.05.002

[13] FLUENT, User's Guide. USA: Fluent, Inc., 2006.

[14] Schmidt, D. P., Nouar, I., Senecal, P. K., Rutland, C. J., Martin, J. K., Reitz, R. D., and Hoffman, J. A., "Pressure-Swirl Atomization in the Near Field," SAE Paper 1999-01-0496, 1999.

[15] O'Rourke, P. J., and Amsden, A. A., "The Tab Method for Numerical Calculation of Spray Droplet Breakup," SAE Paper 872089, 1987.

[16] O'Rourke, P. J., "Statistical Properties and Numerical Implementation of a Model for Droplet Dispersion in Turbulent Gas," *Journal of Computational Physics*, Vol. 83, No. 2, 1989, pp. 345–360. doi:10.1016/0021-9991(89)90123-X

[17] Liu, X. B., and Cheng, L. J., "Effects of Basset History Force on the Motion in a Flow Field," *Journal of Sichuan Institute of Technology*, Vol. 15, No. 2, 1996, pp. 55–63. doi:cnki:ISSN:10005722.0.1996-02-011

[18] Crowe, C. T., Troutt, T. R., and Chung, J. N., "Numerical Models for Two-Phase Turbulent Flows," *Annual Review of Fluid Mechanics*, Vol. 28, Jan. 1996, pp. 11–43. doi:10.1146/annurev.fl.28.010196.000303

[19] Bai, C., and Gosman, A. D., "Development of Methodology for Spray Impingement Simulation," SAE Paper 950283, 1995.

[20] Stanton, D. W., and Rutland, C. J., "Modeling Fuel Film Formation and Wall Interaction in Diesel Engines," SAE Paper 960628, 1996.

[21] Poux, M., Fayolle, P., Bertrand, J., Bridfoux, D., and Bousquet, J., "Powder Mixing: Some Practical Rules Applied to Agitated Systems," *Powder Technology*, Vol. 68, No. 3, 1991, pp. 213–234. doi:10.1016/0032-5910(91)80047-M

[22] Rhodes, M. J., Wang, X. S., Nguyen, M., Stewart, P., and Liffman, K., "Study of Mixing in Gas-Fluidized Beds Using a DEM Model," *Chemical Engineering Science*, Vol. 56, No. 8, 2001, pp. 2859–2866. doi:10.1016/S0009-2509(00)00524-8

[23] Lacy, P. M. C., "Developments in the Theory of Particle Mixing," *Journal of Applied Chemistry*, Vol. 4, No. 5, 2007, pp. 257–268. doi:10.1002/jctb.5010040504

[24] Chaikittisilp, W., Taenumtrakul, T., Boonsuwan, P., Tanthapanichakoon, W., and Charinpanitkul, T., "Analysis of Solid Particle Mixing in Inclined Fluidized Beds Using DEM Simulation," *Chemical Engineering Journal*, Vol. 122, Nos. 1–2, 2006, pp. 21–29. doi:10.1016/j.cej.2006.05.006

[25] Liscinsky, D. S., True, B., and Holdeman, J. D., "Crossflow Mixing of Noncircular Jets," *Journal of Propulsion and Power*, Vol. 12, No. 2, 1996, pp. 225–230. doi:10.2514/3.24017

[26] Liscinsky, D. S., True, B., and Holdeman, J. D., "Experimental Investigation of Crossflow Jet Mixing in a Rectangular Duct," NASA TM-106152, 1993.

[27] Leong, M. Y., McDonell, V. G., and Samuelsen, G. S., "Mixing of an Airblast-Atomized Fuel Spray Injected into a Crossflow of Air," NASA/CR-210467, 2000.

[28] Zhang, H. B., Liu, L., Sun, H. J., and Bai, B. F., "Mixing Behavior of Angled-Injected Centrifugal Spray Droplets in Crossflow," *6th International Symposium on Multiphase Flow, Heat Mass Transfer and Energy Conversion*, MF-30, American Inst. of Physics, College Park, MD, July 2009.

[29] Liu, L., Zhang, H. B., Sun, H. J., and Bai, B. F., "Turbulent Mixing Flow Structure of Spray Droplets in Crossflow," *6th International Symposium on Multiphase Flow, Heat Mass Transfer and Energy Conversion*, MF-21, American Inst. of Physics, College Park, MD, July 2009.

[30] Maxey, M. R., "The Gravitational Settling of Aerosol Particles in Homogeneous Turbulence and Random Flow Fields," *Journal of Fluid Mechanics*, Vol. 174, Jan. 1987, pp. 441–465. doi:10.1017/S0022112087000193

[31] Fung, J., and Perkins, R. J., "Particle Trajectories in Turbulent Flow Generated by True-Varying Random Fourier Modes," *Proceedings Advances in Turbulence 2*, Springer–Verlag, New York, 1989.

[32] Squires, K. D., and Eaton, J. K., "Preferential Concentration of Particles by Turbulence," *Physics of Fluids A: Fluid Dynamics*, Vol. 3, No. 5, 1991, pp. 1169–1178. doi:10.1063/1.858045

J. Oefelein
Associate Editor